Bursting Phenomenon near the Wall in Open-channel Flows and its Simple Mathematical Model

By

Hiroji NAKAGAWA* and Iehisa NEZU*

(Received May 1, 1978)

Abstract

In this paper we propose a new evaluation method for the bursting period, on the basis of the phenomenological consideration that the number of the occurrences of inter-action-like motions should be removed from those of the ejection or the sweep events in the sorted Reynolds-stress fluctuating signals. Then, it is confirmed by this method that the mean bursting period in open-channel flows may be universally expressed by outer rather than inner parameters, and that its probability distribution becomes log-normal, irrespective of the Reynolds and the Froude numbers, as well as the wall roughness.

Next, in order to explain even quantitatively the bursting process or the turbulent structure in the wall region, we propose a simple mathematical model on the basis of the Einstein-Li model and also the knowledge of the bursting-period characteristics obtained above. Though the present model is inherently quasi-two-dimensional and quasi-linear, this model can describe fairly well some distributions of mean-velocity, turbulence intensities and Reynolds stress. In particular, it can satisfactorily explain a sequence of the bursting process.

1. Introduction

Intensive experimental researches on the bursting phenomenon have been performed by making use of visual methods or conditional point-measurements, since it was con-firmed that the bursting process played an essential role for the turbulence-production mechanism near the wall in a turbulent boundary layer,[1] a pipe[2] or open-channel flows.[3] Kline et al.,[1] Corino & Brodkey,[2] Kim et al.,[4] Nychas et al.,[5] Offen & Kline[6],[7] and others found by flow visualization that a sequence of the bursting events such as ejections or sweeps had a quasi-cyclic process. That is to say, it shows a periodic motion on the average in space and time, but not perfectly periodic at one place in time nor at one time in space. For example, Corino & Brodkey[2] presented visual sketches of a sequence of

* Department of Civil Engineering

the bursting events near the wall as shown in figure 1.   They pointed out that there were variations of the sequence, and that all of the steps did not appear all the time or in the exact fashions described, but on the average it proceeded.

Thus, in order to reveal the governing parameters of the bursting phenomenon, it is necessary to investigate its periodic characteristics.   The visual method whereby the bursting period is determined by counting the frequency of occurrences of the coherent motions near the wall visualized on high-speed movie films, is simple and plain.   However, it needs laborious work and more or less involves subjective judgement.

On the other hand, Lu & Willmarth,[8] Brodkey et al.,[9] Nakagawa & Nezu[10] and others have shown that the existence of a sequence of bursting events such as ejections,
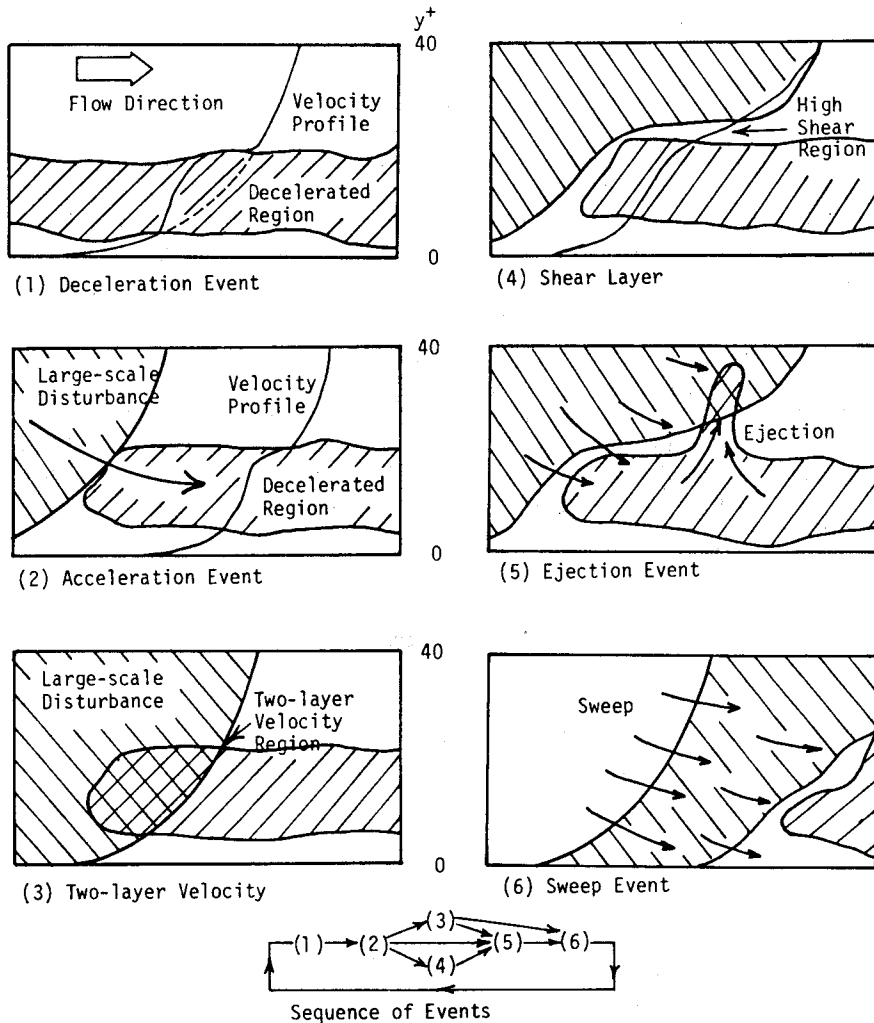

Fig. 1.   Observation of a sequence of the bursting events (*after Corino and Brodkey*).[2]

sweeps and interactions can be also detectable even in the fluctuating velocity signals obtained by hot-wire or hot-film anemometers when a conditional sampling technique is reasonably used. If it is, therefore, possible to establish a reasonable criterion for discriminating the ejections or the sweeps from these velocity signals, the bursting period can be also evaluated easily from the data analysis of point-measurement signals by using a high-speed digital computer. Of course, these results should be compared with the visual data, since it may be fairly difficult to detect accurately the coherent motions extending in space only by one or a few hot-films.

Firstly, Rao et al.[11] estimated the mean bursting period $\bar{T}_B$ from the single-hot-wire signals of streamwise velocity fluctuations $u(t)$ in a boundary layer by using a special criterion for discrimination. They proposed the following experimental results.

$$\bar{T}_B U_*{}^2/\nu = 0.65 \, R_\theta{}^{0.73} \tag{1}$$

$$\bar{T}_B U_{max}/\delta_* \doteqdot 32 \tag{2}$$

where, U_* is the friction velocity, U_{max} is the free stream velocity corresponding to the maximum velocity in an open-channel, R_θ is defined as $R_\theta \equiv U_{max}\theta/\nu$, δ_* is the displacement thickness and θ is the momentum thickness. They found that the mean bursting period could scale with outer rather than inner parameters, as shown in (1) and (2), and that the probability distribution of the bursting period might be log-normal.

Next, Kim et al.[4] found that when the auto-correlation of $u(t)$ reached the re-rise maximum, the lag time τ_0 agreed fairly well with the bursting period evaluated from the visual data. Consequently, they suggested that τ_0 could be regarded as a bursting period $\bar{T}_B$. By these means, Laufer & Narayanan[12] evaluated the mean period of the bursting phenomenon near the viscous sublayer in a boundary layer, and verified that (1) was valid and could be reduced to the following equation by assuming the 1/7-power velocity law:

$$\bar{T}_B U_{max}/\delta \simeq 5 \tag{3}$$

where δ is the boundary layer thickness. Consequently, (1), (2) and (3) are almost the same. ($\bar{T}_B U_{max}/\delta$ becomes nearly equal to 4 from (2) since $\delta/\delta_* = 8$ for the 1/7-power velocity law.) Also, the dependency of the bursting period upon the outer parameter (U_{max} and δ) is confirmed. However, Lu & Willmarth[8],[13] pointed out that these criteria had something unreasonable, and proposed another method described as follows. The fluctuating signals $w'(t) = uv/u'v'$ of the Reynolds stress (where v is the normal fluctuating velocity, $u' \equiv \sqrt{\overline{u^2}}$ and $v' \equiv \sqrt{\overline{v^2}}$) were used as a detection of the coherent motions. The mean period $\bar{T}_e$ of the ejection motion was evaluated from $w'(t)$ in the ejection event ($u < 0$, $v > 0$), when the discrimination level was set at the value of ($4.0 \sim 4.5$) where the sweeps almost disappeared. The mean period $\bar{T}_s$ of the motion was also evaluated in the same manner. Their results agreed fairly well with the visual data, or

(3), and this evaluation method might become more reasonable than previous methods. Indeed, Sabot & Comte-Bellot[14] evaluated the bursting period in a pipe flow by this method.

In the light of the above, the present study is to propose another reasonable evaluation method of the bursting period, and investigate the periodic characteristics of the bursting phenomenon in open-channel flows. Then, on the basis of the knowledge obtained from these investigations, a simple mathematical simulation model will be proposed in order to explain the bursting phenomenon or the turbulence characteristics quantitatively.

2. Experimental equipment and data analysis

Two groups of experiments on two-dimensional fully developed turbulent flows in an open channel were conducted in a tilting flume 15 m long, 50 cm wide and 30 cm deep. One group was a lower-velocity one (the Reynolds number $Re \equiv U_m h/\nu$, where U_m was the mean velocity and h was the flow depth. It was nearly equal to 1×10^4) which consisted of four kinds of bed roughness; that is, one smooth lucite bed (Case A) and three roughness beds (Cases B, C and D). The scope of this group was described in our previous paper.[10] The other was a higher-velocity group ($Re = 3.2 \times 10^4$) on a smooth bed for five different kinds of the Froude number $Fr = U_m/\sqrt{gh}$. The hydraulic parameters for each run are shown in Table 1. It was expected that the effects of roughness, the Froude and the Reynolds numbers upon the bursting phenomenon would be observed by these nine tests.

Table 1. Hydraulic parameters for experiments and the results of the mean bursting period.

Case	h (cm)	U_{max} (cm/s)	U_m (cm/s)	U_* (cm/s)	$Re \equiv \dfrac{U_m h}{\nu}$ ($\times 10^4$)	$R_* \equiv \dfrac{U_* h}{\nu}$ ($\times 10^2$)	$Fr \equiv \dfrac{U_m}{\sqrt{gh}}$	k_s^+	$\dfrac{\bar{T}_e U_{max}}{h}$	$\dfrac{\bar{T}_s U_{max}}{h}$	$\dfrac{\bar{T}_e U_*^2}{\nu}$	$\dfrac{\bar{T}_s U_*^2}{\nu}$
A-1	7.77	16.8	14.8	0.810	1.09	5.98	0.170	≒0	2.60	2.21	74.8	63.6
B-1	7.94	17.7	15.5	0.895	0.98	5.66	0.175	9.1	2.41	2.06	69.0	59.0
C-1	7.83	15.7	13.2	0.989	0.98	7.37	0.150	48.0	1.90	1.57	88.3	72.9
D-1	7.63	17.2	13.9	1.267	0.86	8.32	0.160	136.2	2.43	1.96	148.8	120.0
G-1	8.01	48.3	40.1	2.152	3.03	16.3	0.455	≒0	1.82	1.87	132.0	135.8
G-2	5.49	73.2	58.5	3.138	3.23	17.6	0.798	≒0	1.61	1.43	121.0	107.9
G-3	4.14	101.8	77.2	3.748	3.27	15.9	1.21	≒0	1.75	1.68	102.4	98.3
G-4	3.15	118.6	101.2	4.711	3.19	14.9	1.82	≒0	2.26	2.04	133.8	120.7
G-5	2.20	169.4	144.8	6.162	3.27	13.9	3.12	≒0	2.79	2.31	141.0	116.8

The streamwise and normal components of the instantaneous velocity were measured by using a set of constant-temperature anemometers with a DISA type 55A89 dual-sensor hot-film probe. The output signals of the anemometers were recorded in analog form by using an FM tape recorder, and then were reproduced for conversion to digital form. It is important how to determine the number N of samples and the sampling frequency f at any measuring point on performing an analog-to-digital conversion. The maximum cutoff wave-number k_∞ is given by

$$L_x \cdot k_\infty \simeq \pi \cdot f \cdot h / U \tag{4}$$

If $L_x \cdot k_\infty$ is over about a hundred, the spectral analysis becomes possible at least to the extent of the inertial subrange.[15] Thus, the sampling frequency f was chosen in each run so as to satisfy this analytical condition. The total sampling time $T = N/f$ is given in the following by using (3):

$$\frac{T}{\bar{T}_B} \simeq \frac{\pi}{500} \left(\frac{U_{max}}{U} \right) N \sim \frac{N}{100} \tag{5}$$

Though the larger the sample size N is, the better the accuracy of data analysis becomes, $N=5000$ was chosen in this study because of the limitation of our computer technique. Thus, this sample size ($T \sim 50 \bar{T}_B$) may be comparatively small but it includes the characteristics of bursting phenomenon from this data analysis.

Next, several tests of flow visualization were also conducted by using a hydrogen-bubble method in order to supplement the hot-film data. Especially, the behaviour of high- and low-speed streaks was investigated by visualization of the instantaneous velocity profiles in a horizontal plane. The details of this visual method and its results are given in another paper of ours.[16]

3. Periodic characteristics of the bursting phenomenon

3.1 Discrimination criterion and definition of the bursting period

The instantaneous Reynolds-stress signals $w(t) \equiv uv/\overline{uv}$ are reasonably used as discriminating information, since they are directly related to the mechanism of turbulence-production, namely the bursting phenomenon.[10] Now, $w(t)$ is conditionally divided into four events: $w_1(t)$ when $u>0$ and $v>0$ (outward interaction), $w_2(t)$ when $u<0$ and $v>0$ (ejection), $w_3(t)$ when $u<0$ and $v<0$ (inward interaction) and $w_4(t)$ when $u>0$ and $v<0$ (sweep). Obviously,

$$w(t) = w_1(t) + w_2(t) + w_3(t) + w_4(t) \tag{6}$$

Two typical examples of the conditionally sampled signals $w_i(t)$ ($i=1\sim4$) measured at $y^+=38$ (wall region) and $y/h=0.193$ (equilibrium region) over a smooth bed (Case
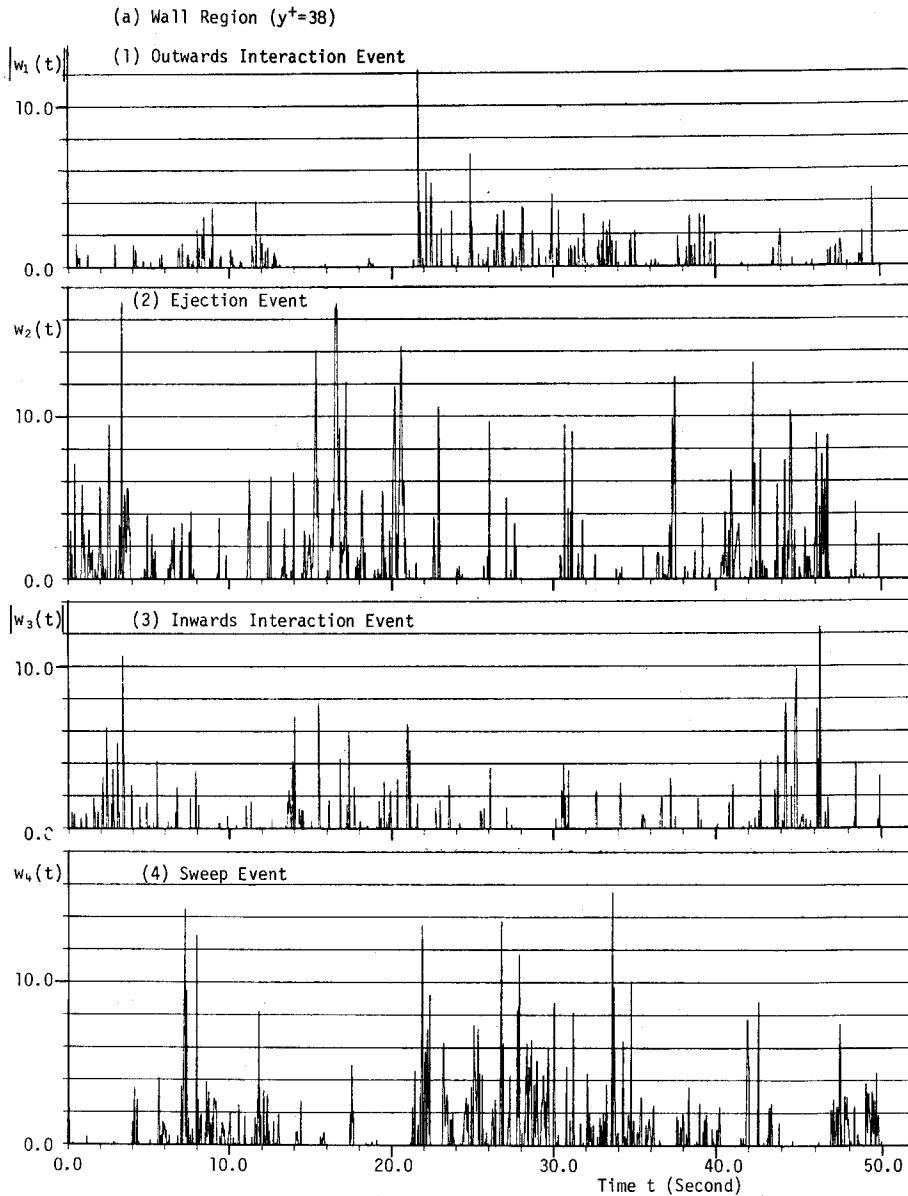
Fig. 2. (a)   Fluctuating signals of Reynolds stress at each event in the wall region.

A-1) are shown in figure 2, (a) and (b), where the structure of their Reynolds stress has been already made clear theoretically and experimentally.[10]   It is confirmed that the Reynolds stress fluctuations $w(t)$ are very intermittent, and especially that the ejections and sweeps generate turbulence violently in the form of a very sharp pulse.   Such a behaviour has been also visualized by many other researchers[2],[3],[4],[5].

(b) Equilibrium Region (y/h=0.193)

(1) Outwards Interaction Event

$|w_1(t)|$

(2) Ejection Event

$w_2(t)$

(3) Inwards Interaction Event

$|w_3(t)|$

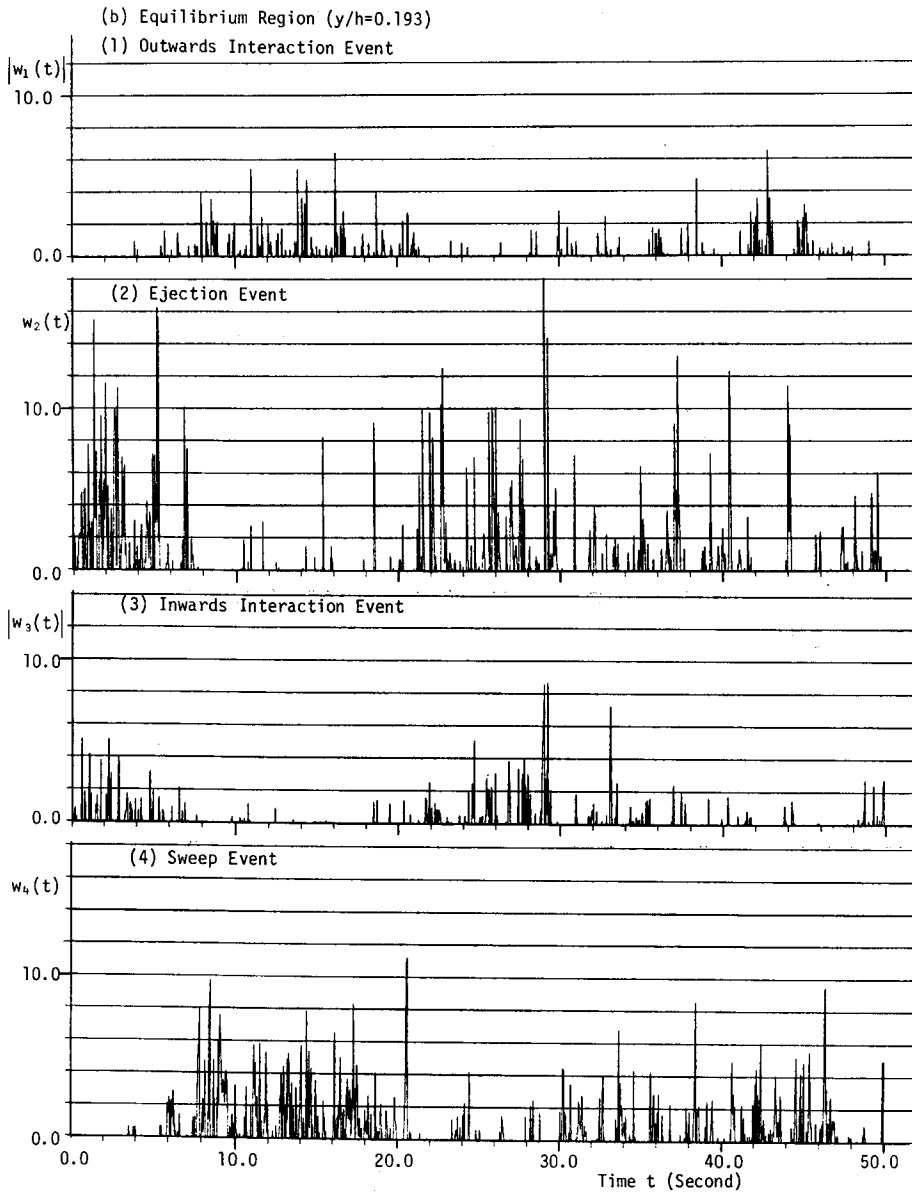(4) Sweep Event

$w_4(t)$

Time t (Second)

Fig. 2. (b)   Fluctuating signals of Reynolds stress at each event in the equilibrium region.

The hole size H for the division of the bursting events is introduced as a discrimination level of the ejection or sweep motions.[10]   Assuming that each event motion with a certain level H occurs when $|w_i(t)|$ reaches or exceeds level H, its mean period T_i ($i=1\sim4$) is obtained by counting the number N_i of the occurrences in the total observing time T, as follows:

$$T_i(H) = T/N_i \quad (i=1 \sim 4) \tag{7}$$

For example, figure 3 shows the variation of the mean period $T_2(H)$ of an ejection event normalized by outer parameters (U_{max} and h) for a smooth bed. Since T_2 is a monotonously increasing function of H, the mean period $\bar{T}_e$ of the ejection motion which can be observed visually, that is, an event (5) in figure 1, cannot be determined from figure 3 without providing a discrimination criterion. According to the Lu & Willmarth method, as mentioned previously, $\bar{T}_e U_{max}/h$ becomes (4~10) since the level H is about 10, at which the contributions of the sweeps almost disappear.[10] This range of $\bar{T}_e$ is too large to know the effects of hydraulic parameters such as Re, Fr and the wall roughness upon the bursting period systematically.

Now, it may be noticed in figures 3 and 4 that T_2 shows a nearly linear increase with H when $H \lesssim 5$, and a more remarkable increase when $H \gtrsim 5$ although the slope of $T_2(H)$ increases more or less continuously. This tendency of $T_2(H)$ may be related to the fact that the interaction events scarcely contribute to the production of Reynolds stress when level H reaches about 5.[10] This suggests that the ejection signals $w_2(t)$ or the sweep signals $w_4(t)$ with $H \lesssim 5$ contain a part of the interaction motions corresponding to the events (1)~(4) in figure 1. This suggestion may be also inferred from the results of a conditional sampling technique, as shown by the following.

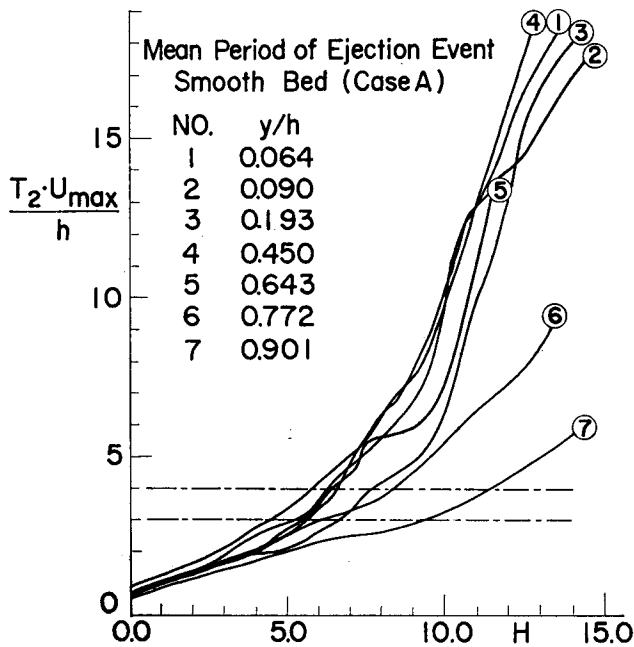Since a coherent motion of bursting phenomenon is visualized in a form of the

Fig. 3. Mean period T_2 of ejection event with H.

Smooth Bed(Case A-1)
O :from present method
● :From Kim et al.'s method
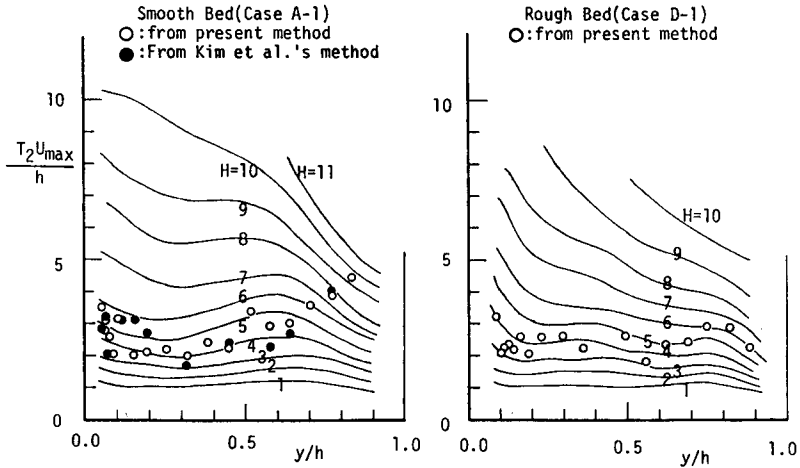
Rough Bed(Case D-1)
O :from present method

Fig. 4.   Mean period T_2 of ejection event against y/h as a parameter of H.

streamwise velocity fluctuations $u(t)$ instead of the Reynolds stress fluctuations $w(t)$, a trigger level u_L is set for $u(t)$.   Then, denoting $t=0$ when $|u(t)/u'|$ crosses a special trigger level u_L in an increasing direction, $w_2(t)$ has been ensemble-averaged.   Figure 5, (a) and (b), shows the behaviours of the ensemble-averaged ejections with three cases of trigger levels; that is, $u_L=0.5$, 1.0 and 1.5, in the wall and the equilibrium regions, respectively (corresponding to figure 2).   The existence of the coherent motion is not recognized at $u_L=0.5$, but if u_L is set at 1.0, $w_2(t)$ has a large peak immediately after
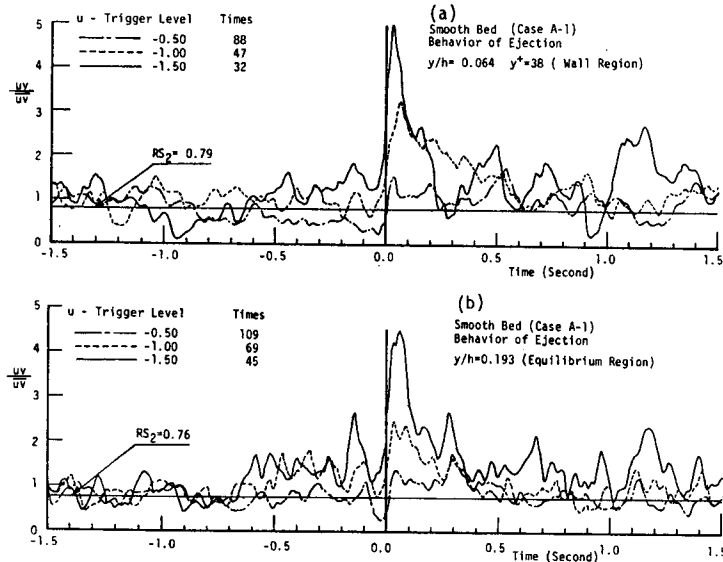
Fig. 5.   Behaviour of ejection motions detected at the trigger level u_L in the wall and equilibrium regions.

$u(t)/u'$ reaches a level of -1.0, and a larger peak appears at $u_L = 1.5$. The ensemble-averaged sweeps have shown a similar trend as do the ejections. The fact that the ejection or the sweep motions can be detected in $w(t)$ when $u_L \geq 1.0$, agrees well with the point-measurement data given by Lu & Willmarth.[8] Since $u_L = (1.0 \sim 1.5)$ corresponds roughly to $H \simeq 5$,[15] the energetic ejection or sweep motions which can be observed visually, corresponding to event (5) or (6) in figure 1, would be able to be detected from the conditionally sorted signals $w_2(t)$ or $w_4(t)$ when H is set at about 5.

From the above phenomenological considerations, the contributions of the interaction motions should be removed from the sequence of the bursting process in order to evaluate the period of only the ejections or sweeps. However, there is at present quite a lack of knowledge about the contributions of the interaction-like motions which may be contained in the signals of $w_2(t)$ or $w_4(t)$. Hence, we now propose a tentative assumption that the interaction-like contributions may be of the same order as those of the interaction event signals $w_1(t)$ or $w_3(t)$, since the contributions of $|w_i(t)| \lesssim 5$ might be roughly equal to each other, owing to a detection of old-born or new-born small bursting motions. By assuming that the number N_{in} of occurrences of these interaction-like motions with a level of H is roughly given by an average of those of two interaction events: that is, $N_{in} = (N_1 + N_3)/2$, the revised bursting period is defined as follows:

$$\hat{T}_2 \equiv T/(N_2 - N_{in}) \text{ (Ejections)}, \quad \hat{T}_4 \equiv T/(N_4 - N_{in}) \text{ (Sweeps)} \tag{8}$$

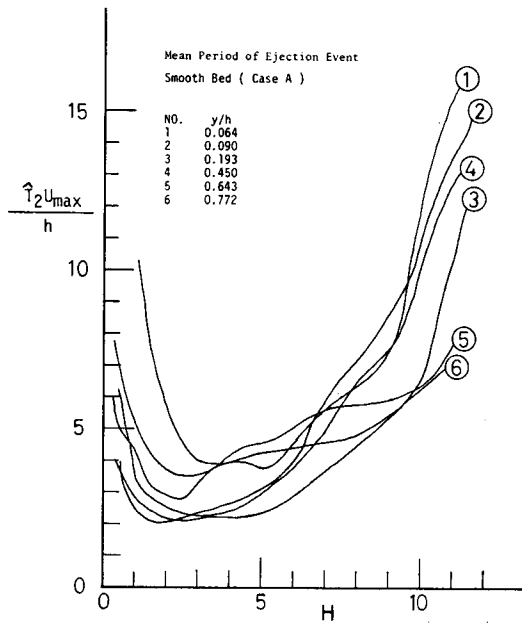$\hat{T}_2 U_{max}/h$ is shown against H in figure 6 for the case corresponding to figure 3. When

Fig. 6. Mean period $\hat{T}_2$ of ejection event where the interaction-like motions are subtracted.

H is small, $\hat{T}_2 U_{max}/h$ is large owing to the strong cancellation effect of the interaction-like motions, as mentioned above. Because the interaction-like motions disappear gradually as H increases, this cancellation effect becomes weaker, and consequently $\hat{T}_2$ approaches T_2. Thus, we try to tentatively define the mean period of the ejections $\bar{T}_e$ and the sweeps $\bar{T}_s$ as the minimum value of $\hat{T}_2(H)$ and $\hat{T}_4(H)$, respectively, because it may be considered that the interaction-like contributions almost disappear at this minimum point. Since the minimum value of $\hat{T}_2(H)$ or $\hat{T}_4(H)$ remains stationary even when H varies to some extent, $\bar{T}_e$ or $\bar{T}_s$ can be determined uniquely, and therefore this evaluation method may be well-defined as compared with previous methods. Some results of $\bar{T}_e$ evaluated from this method have been plotted in figure 4, together with the data of the bursting period $\bar{T}_B$ obtained by Kim et al's method, although it was difficult to evaluate $\bar{T}_B$ accurately, except when near the wall. The values of $\bar{T}_e$ had a good agreement with those of $\bar{T}_B$ and our visual data.[16] Therefore, our tentative evaluation method of the bursting period seems to be fairly reasonable.

3.2 Bursting period and its probability characteristics

The evaluated values of $\bar{T}_e$ and $\bar{T}_s$ in the wall and equilibrium regions $(y/h \lesssim 0.6)$ for all experimental runs are shown in figure 7, normalized by the outer parameters. Although there are some scatterings in these data, $\bar{T}_e U_{max}/h$ and $\bar{T}_s U_{max}/h$ are approximately constant for any y/h, irrespective of the hydraulic conditions. Their average values against y/h for each run are described in table 1, and a relation may be obtained as follows:

$$\frac{\bar{T}_e \cdot U_{max}}{h} \simeq \frac{\bar{T}_s \cdot U_{max}}{h} \simeq (1.5 \sim 3.0) \tag{9}$$

(9) shows the same order as (3) or Lu & Willmarth's results in a boundary layer,[8] though a quantitative comparison among these data cannot be done reasonably because of the differences of the flow conditions and the evaluation methods. It should be noticed that the ejection period $\bar{T}_e$ becomes nearly equal to the sweep period $\bar{T}_s$, as pointed out by Lu & Willmarth.[8] This means that there exists, on an average, at least one each of ejection and sweep motions in a bursting process. Consequently, the bursting period $\bar{T}_B$ can be identified with the ejection or sweep one, that is, $\bar{T}_e \simeq \bar{T}_s \simeq \bar{T}_B$.

The inner-parameter description $\bar{T}_B U_*^2/\nu$ of the bursting period is shown in figure 8 against the Reynolds number R_θ (for a boundary layer) or $R_* \equiv h U_*/\nu$ (for an open channel). The authors' visual data, which were evaluated from the periodic characteristics of the time-line of the hydrogen-bubble in the wall region,[16] were also plotted in this figure in order to supplement the data for the lower Reynolds number. Our results in open-channels seem to be similar to those in boundary layers that satisfy (1) very well as mentioned in chapter 1. Also, if R_θ is replaced by R_*, (1) may be approximately

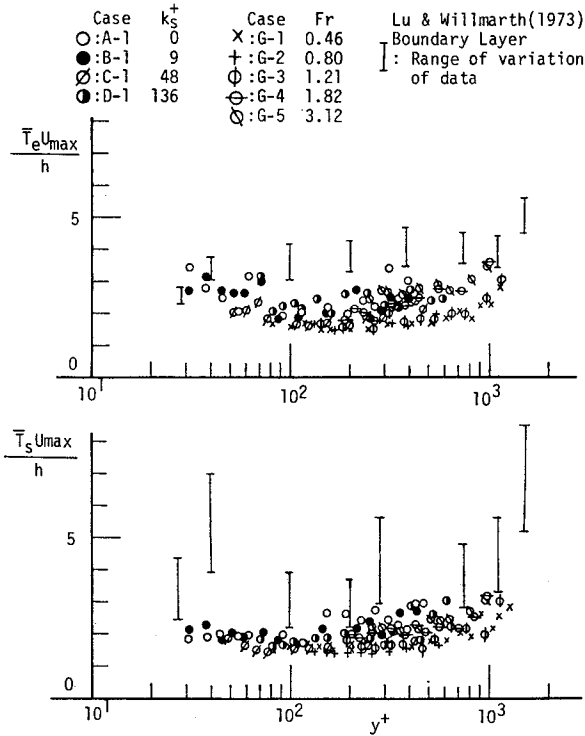| Case	k_s^+		Case	Fr	Lu & Willmarth(1973)
○:A-1	0		×:G-1	0.46	Boundary Layer
●:B-1	9		+:G-2	0.80	I : Range of variation
⊘:C-1	48		⏀:G-3	1.21	of data
◑:D-1	136		⊖:G-4	1.82	
			⊗:G-5	3.12	

Fig. 7.   Mean bursting period normalized by the outer parameter as a function of y^+.

valid even in open channels.

From the previous and present investigations, it may be concluded that the bursting period in the wall and equilibrium regions of open-channel flows can scale with the outer
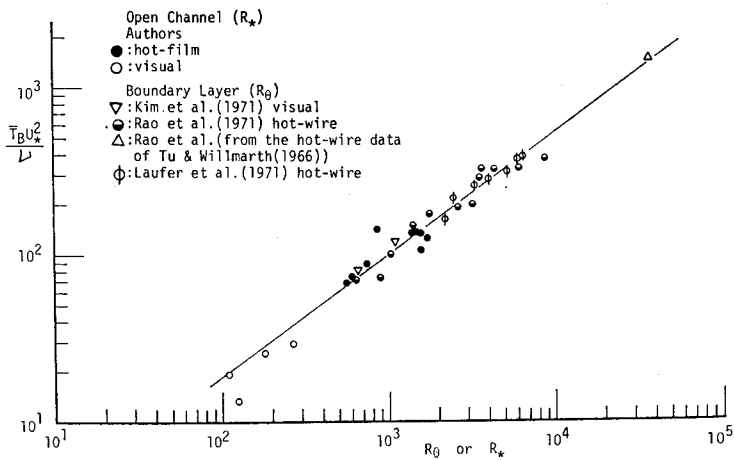
Fig. 8.   Mean bursting period normalized by the inner parameter as a function of the Reynolds number.

valid even parameters (U_{max} and h) rather than the inner parameters (U_* and ν/U_*), irrespective of Re, Fr and the wall roughness. This is also supported by the noticeable fact that the wall roughness scarcely influences the bursting period, while this effect can be noticed clearly in the bursting process near the wall as pointed out by the authors.[10]

Next, the probability distribution $P_T(T)$ of the bursting period T will be discussed.[*] The experimental values of $P_T(T)$ can be obtained from figure 2, since the hole size level H corresponding to the mean period $\bar{T}_e$ or $\bar{T}_s$ is determined easily from figures 3 or 4. According to the suggestion of Rao et al.,[11] the data of the probability distribution of $\sigma_0^{-1} \log (T/T_0)$ have been plotted in a normal-probability paper, where $\log T_0 \equiv \overline{\log T}$ and $\sigma_0 \equiv \{\overline{(\log T/T_0)^2}\}^{1/2}$. Some examples of these results for smooth and rough beds are shown in the right and left sides of figure 9, respectively. The straight line described in this figure is a log-normal distribution which is written by

$$P_T(T) = \frac{(\log e)}{\sqrt{2\pi}\,\sigma_0 T} \exp\left\{-\frac{1}{2}\left(\frac{1}{\sigma_0}\log T/T_0\right)^2\right\} \tag{10}$$

Though there is a little scattering in our hot-film data, these data have a good agreement with (10), as well as the visual data obtained by Kim et al.[4] Consequently, it is confirmed that the probability of the bursting period can be described approximately by a log-normal distribution, that is (10), irrespective of Re, Fr and the wall roughness.

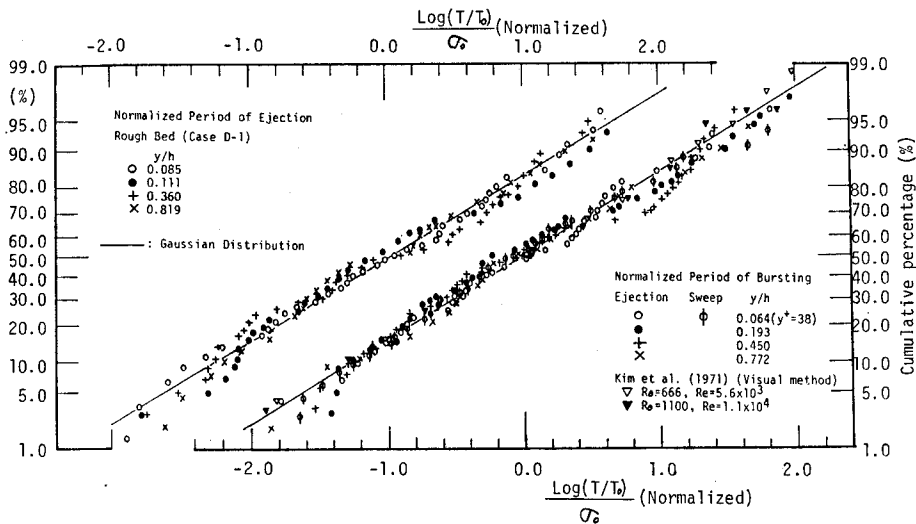Then, the following equation can be obtained easily from (10).

Fig. 9. Normalized probability distributions of the bursting period.

---

[*] When it isn't necessary to distinguish between the ejection period T_e and the sweep period T_s, these suffixes will be omitted in the following explanations. The mean value $\bar{T}$ of the bursting period can be represented for $\bar{T}_e \simeq \bar{T}_s \simeq \bar{T}_B$.
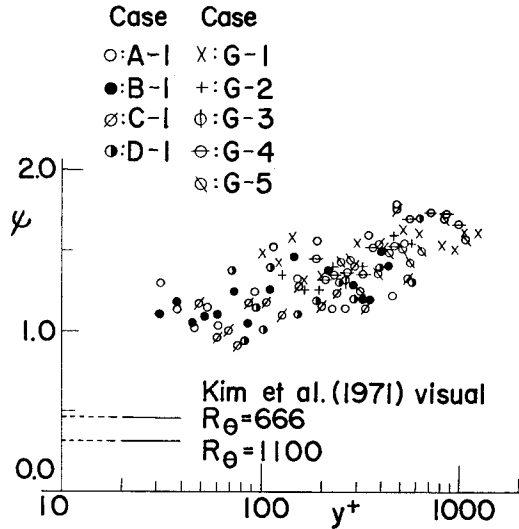
Fig. 10. Coefficient of variation of the bursting period.

$$\int_0^\infty T^i P_T(T) dT = T_0^i \cdot \exp\left(\frac{i^2}{2K^2}\right), \quad K \equiv (\log e)/\sigma_0 \tag{11}$$

Denoting $T_B = \bar{T}$, $\sigma_B = (\overline{(T-\bar{T})^2})^{1/2}$ and $\psi = \sigma_B/T_B$,

$$\left.\begin{array}{l} \sigma_0 \equiv (\log e)/K = (\log e)\sqrt{\ln(1+\psi^2)} \\ T_0 \equiv \gamma T_B, \quad \gamma \equiv (1+\psi^2)^{-1/2} \end{array}\right\} \tag{12}$$

Thus, if the mean value T_B and its coefficient ψ of variation are known, (10) can be determined as a probability distribution of the bursting period. The experimental values of ψ for the ejection period are shown in figure 10, and similar results have been also obtained for the sweep period. As concerns our hot-film data, the values of ψ near the wall are nearly constant: that is, $\psi \simeq (1.0 \sim 1.5)$, while the visual data of Kim et al. show $\psi \simeq 0.5$. Though at present, while it is difficult to explain the cause of this difference between the hot-film and visual data, the former may be apt to be accompanied by a kind of unevenness involved in the point-measurements of the coherent motions which extend in space. Consequently, the hot film data are probably evaluated larger than the visual data.

3.3 Dependence of the bursting phenomenon upon the inner and outer parameters

For the present, from the previous and present experimental data, we can approve the opinion that the bursting period may be controlled by the outer rather than the inner parameters. Consequently, the turbulent structure in the wall region of an open-channel flow may be characterized not only by the inner parameter,[15] but also by the outer para-

meter that characterizes the free-surface, region, which have been already recognized in a boundary layer flow.

Now, the streamwise, the vertical and the transverse spatial scales of this coherent motion are denoted by λ_1, λ_2 and λ_3, respectively. Since the mean streamwise spatial scale $\bar{\lambda}_1$ is nearly equal to $\bar{T}_B \cdot U_c$, where U_c is the convection velocity and $U_c \simeq U_m \simeq 0.9 U_{max}$,[15] it becomes from (9) as

$$\bar{\lambda}_1/h \simeq (1.5 \sim 3.0) \qquad \text{(open-channel)} \tag{13}$$

as well as $\bar{\lambda}_1/\delta \simeq 4$ in a boundary layer, as shown by Hinze.[17] The mean vertical spatial scale $\bar{\lambda}_2$ is considered to be below the wall region thickness, that is, $\bar{\lambda}_2^+ < 100$. In particular, it is suggested from the visual observation[2] that $\bar{\lambda}_2^+ \lesssim 50$, where the coherent motions appear most violently. The mean transverse spatial scale $\bar{\lambda}_3$ may be able to be identified with the spacing between the high and low speed streaks which were found by Kline et al.[1] It was confirmed by our visual observations[16] that

$$\bar{\lambda}_3^+ \simeq 100 \tag{14}$$

in open channels, which coincided with the data in boundary layers.

From the results obtained above, it is deduced that a typical eddy with coherent motions near the wall may depend upon both the inner and outer parameters. Consequently, the eddy model qualitatively described by Hinze[17] in figure 11 may fairly reasonably explain the mechanism of the bursting phenomenon, as will be shown later. Furthermore, we have found a log-normal distribution of the probability of λ_3,[16] as well
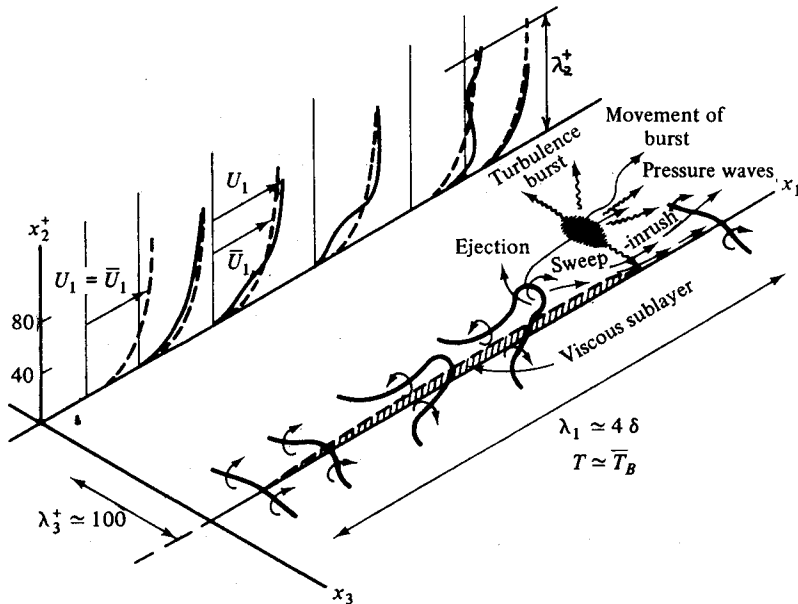

Fig. 11. Conceptual model of the turbulence near the wall during a 'cyclic' process (*after J. O. Hinze*).[17]

as $\lambda_1 \simeq T \cdot U_e$ (refer to (10)).   In other words, it seems that the bursting phenomenon has self-consistently the characteristic of a log-normal distribution while it is controlled by both the inner and outer parameters.

Hence, a closer interrelation between the wall and the free-surface regions in an open channel corresponding to the inner and the outer layers in a boundary layer is suggested more than had been previously expected.

Incidentally, Laufer & Narayanan[13] deduced that the bursting phenomenon near the wall might be caused by the bulge motions near the boundary layer edge, but we cannot find any bulge motions in an open-channel flow.   We infer here that there may exist a close relation between the bursting mechanism and the breakdown mechanism of the largest-scale eddy with scale L_0.   If the Strouhal similarity might be valid for both mechanisms, the following relation could be obtained.

$$T_B U_{max}/h \simeq (St)^{-1} (L_0/h) \tag{15}$$

where, St is the Strouhal number and it may be now tentatively roughly equal to 0.2, with an assumption that the breakdown of this eddy would be roughly similar to that of the Karman-vortex.   Then, (15) may coincide roughly with (3) or (9) since $L_0/h \simeq 0.8$.[15]

Hence, it may be fairly well asserted from the visual observations of figure 2 that the breakdown of the largest-scale eddy is intermittent, and then generates most of the turbulent energy or the Reynolds stress.   On the other hand, as indicated by Sandborn,[18] the breakdown of the smallest-scale eddy is also intermittent, and then dissipates most of the turbulent energy.

Among the evaluation methods of the bursting period mentioned previously, the methods of Rao et al.[11] and Ueda & Hinze[19] are based on a microscale intermittency, while the methods of Kim et al.,[4] Lu & Willmarth,[8] the present authors as well as the visual method are based on a macroscale intermittency.   Since almost the same characteristics of the bursting period have been evaluated from these two different methods, it is inferred that the breakdown of a macroscale eddy may have a close relation and interaction with that of a microscale eddy, and that the turbulent structure may be essentially characterized by both the macro- and micro-scales.   Consequently, an energy cascade process in which the turbulent energy of macroscale eddies is gradually transfered to that of microscale eddies would be more complicated than we have previously understood.   Therefore, assuming that there exists a self-similarity in the breakdown of eddies of this cascade process, log-normal characteristics of the bursting process or the coherent motion reported here could be explained by the eddy model of Gurvich & Yaglom[20].   Thus, it is suggested that the bursting phenomenon may be closely related to the breakdown mechanism of both the macro-and micro-scale eddies, and further investigations will be needed in order to make clear the above suggestions.

4. Simply mathematical modelling of the bursting phenomenon

4.1 Brief recapitulation of previous eddy models and present object

Even before the existence of the bursting phenomenon was discovered clearly by Kline et al.,[1] there had been already several attempts to describe the mechanism of the turbulence production near the wall by suitable turbulent eddy models, among which a horseshoe vortex model proposed by Theodorsen[21] and a renewal model of the viscous sublayer proposed by Einstein & Li[22] should be still noteworthy, as mentioned in the following.

Willmarth & Tu[23] proposed an 'average model of vortex line' in order to qualitatively explain the pressure-velocity correlations near the wall, from which the existence of the bursting phenomenon might be inferred. Next, Kline et al.[1] offered an eddy model by which the mechanism of wall-turbulence production could be reasonably explained. Both of these eddy models are very similar to Theodorsen's horseshoe vortex model. We can recognize for the present that such an eddy model might be most suitable for a qualitative explanation of the bursting process, as shown in figure 11. As a fact, Black[24] formulated this horseshoe vortex model phenomenologically, after which he could successfully explain several turbulence characteristics quantitatively.

In order to quantitatively describe the turbulent structure in the equilibrium region ($y^+ > 100$), we[25] also proposed a Π-eddy model whereby a horseshoe vortex model was simplified by assuming that some of the horseshoe vortices in the wall region, shown in figure 11, survived without the vortex-breakdown during their development, even in the region of $y^+ > 100$, and also attained the equilibrium state of turbulent energy, i.e. the balance between the production and the dissipation. A Π-eddy consists of a primary motion with an elliptic steady circulation in the vortex axis, and a secondary motion with a perturbation of its vortex tube due to the vortex-stretching effect. The spectral analysis of Π-eddies with various scales gave a remarkable result whereby the section of their vortex tubes was distorted by about 60 percent in the streamwise direction, and the angle of the inclination of their vortex tubes toward the wall was uniformly developed up to about 80 degrees. The following relations about the turbulent intensities were obtained from an equilibrium condition of turbulent energy.[15]

$$u'/U_* = D_1 \cdot \exp(-y/h) \tag{16a}$$

$$v'/U_* = D_2 \cdot \exp(-y/h) \tag{16b}$$

$$w'/U_* = D_3 \cdot \exp(-y/h) \tag{16c}$$

where, D_1, D_2 and D_3 are the experimental constants. Since the Π-eddy model predicted that $v'/u' = 0.55$ and $w'/u' = 0.69$, we could obtain $D_2 = 1.27$ and $D_3 = 1.59$ by using the experimental value $D_1 = 2.3$[15]. Then, it was confirmed that (16) agreed fairly well with

the observed values in the region of $y^+>50$, and consequently that the Π-eddy model could explain quantitatively the turbulent structure in the equilibrium region. However, the Π-eddy model is not applicable to the wall region of $y^+<50$ where the bursting phenomenon occurs remarkably, because a horseshoe vortex in this region is under development, that is, a non-equilibrium state.

Hence, with a view to quantitatively describing the bursting process, we now propose a simple mathematical model to simulate this process on the basis of the Einstein-Li model and the knowledge obtained in the previous chapter.

4.2 Formulation of a renewal model

We consider an idealized model of the bursting process, which is called a renewal model, because it is most essential to take account of its periodic characteristics. We can divide a period T of the bursting phenomenon into two duration intervals: one is the built-up or developing duration T_1, and the other is the breakdown duration T_2 of the coherent vortex motion, that is, $T=T_1+T_2$. The ejection motion occurs in the breakdown duration T_2, and both the sweep and the interaction motions occur in the built-up duration T_1, since the former is swept literally by the latter and a new horseshoe vortex is born again. For convenience, the beginning of a sweep motion is here denoted as $t=0$, and then a sequence of the bursting process is considered to be a cyclic motion of sweep-interaction-ejection-sweep.

Let $\tilde{\boldsymbol{u}}_1=(\tilde{u}_1, \tilde{v}_1)$ and $\tilde{\boldsymbol{u}}_2=(\tilde{u}_2, \tilde{v}_2)$ be the instantaneous velocities during T_1 and T_2, respectively. The eddy-viscosity might be infinitely smaller in the built-up duration and infinitely larger in the breakdown duration than the molecular-viscosity since much of the Reynolds stress is generated by the breakdown of the horseshoe vortex, i.e. ejection motion. Consequently, assuming that the nonlinear coupling effect and the pressure fluctuation effect are negligible during the built-up time, the Navier-Stokes equation which controls the coherent motion in this duration can be approximated by using the boundary layer theory since $\lambda_2^+<\lambda_3^+\ll\lambda_1^+$ (see **3.3**), as follows:

$$\frac{\partial\tilde{u}_1}{\partial t}=\nu\frac{\partial^2\tilde{u}_1}{\partial y^2} \tag{17}$$

The boundary conditions are

$$\tilde{u}_1=0 \text{ at } y=0, \text{ and } \tilde{u}_1=U_0 \text{ at } y\rightarrow\infty \tag{18}$$

where U_0 is the main stream velocity outside the wall region.

Since the distorted velocity distribution of an ejection motion may be swept due to the stress-relieved mechanism and restored to a uniformly accelerated velocity, as observed in figure 1, the initial condition can be idealized by

$$\tilde{u}_1=U_0 \quad (y>0) \quad \text{at } t=0 \tag{19}$$

Then, the solution of (17) with the conditions of (18) and (19) reads

$$\tilde{u}_1 = \frac{2U_0}{\sqrt{\pi}} \int_0^\Theta e^{-x^2} dx \equiv U_0 \, \text{erf} \, \Theta \tag{20}$$

where, $\Theta \equiv y/(2\sqrt{\nu t})$ and erf Θ is the error-function of Θ. (20) was firstly obtained by Einstein & Li,[22] and it forms the origin of the present model. On the other hand, Black[24] adopted Cole's logarithmic law, i.e. $\tilde{u}_1 = U_* (\kappa^{-1} \ln y^+ + 5.1)$ as the initial condition of (17), and then he obtained a more complicated solution than (20). Though this initial condition seems to be more suitable for the actual phenomenon than (19), as seen from figure 1,[2,3] we do not adopt the Black solution here because it is too intricate to go on calculating further.

Now, making the axis transformation to $\partial/\partial t = -U_c \partial/\partial x$ (Taylor's frozen hypothesis) where U_c is the convection velocity of a horseshoe vortex, and using the equation of continuity, we can obtain

$$\tilde{v}_1 = -\int_0^y \frac{\partial \tilde{u}_1}{\partial x} dy = -\frac{1}{a} \sqrt{\frac{\nu}{\pi t}} \{1 - \exp(-\Theta^2)\} \tag{21}$$

where, $a \equiv U_c/U_0$ is $(0.7 \sim 0.8)$ according to the previous experiments.[17]

Next, because the mechanism of the vortex-breakdown is not sufficiently evident, $\tilde{\boldsymbol{u}}_2 = (\tilde{u}_2, \tilde{v}_2)$ is evaluated here by introducing a simplified idea. It is considered that $\beta \equiv T_2/T_1$ is infinitesimal, i.e. $\beta \ll 1$, since the vortex-breakdown or the ejection motion occurs in very short time, as shown in figure 2. Then, $\tilde{u}_1(t = T_1)$ is renewed into $\tilde{u}_1(t = T) \equiv \tilde{u}_1(t = 0)$ in a very short time. Consequently, the average of both $\tilde{u}_1(t = T_1)$ and $\tilde{u}_1(t = T)$ can be represented as $\tilde{u}_2 (T_1 \leq t \leq T)$. We can also obtain $\bar{\tilde{v}}_2 = -\bar{\tilde{v}}_1/\beta$ since the average velocity $V \equiv \bar{\bar{v}} = (T_1 \bar{\tilde{v}}_1 + T_2 \bar{\tilde{v}}_2)/T$ must always be zero in an open-channel flow. Furthermore, $\tilde{v}_2$ may be closely identified with $\bar{\tilde{v}}_2$ for $\beta \ll 1$. Then,

$$\tilde{v}_2 \doteqdot -\bar{\tilde{v}}_1/\beta \tag{22}$$

From the above simplification, the following relations can be obtained by using $\beta \ll 1$.

$$\left. \begin{array}{l} U \equiv \bar{\tilde{u}} = \dfrac{1}{T}\left(\displaystyle\int_0^{T_1} \tilde{u}_1 dt + \int_{T_1}^T \tilde{u}_2 dt \right) \doteqdot \dfrac{1}{T} \int_0^T \tilde{u}_1 dt \\[4mm] V \equiv \bar{\tilde{v}} = 0 \end{array} \right\} \tag{23}$$

$$\left. \begin{array}{l} u'^2 \equiv \overline{(\tilde{u} - U)^2} \doteqdot \dfrac{1}{T} \displaystyle\int_0^T \tilde{u}_1^2 dt - U^2 \\[4mm] v'^2 \equiv \overline{(\tilde{v} - V)^2} \doteqdot \dfrac{1}{(1+\beta)} \left\{ \dfrac{1}{T_1} \displaystyle\int_0^{T_1} \tilde{v}_1^2 dt + \dfrac{1}{\beta} (\bar{\tilde{v}}_1)^2 \right\} \end{array} \right\} \tag{24}$$

$$\overline{uv} = \{ \overline{(\tilde{u}_1 - U) \cdot \tilde{v}_1} + \beta \overline{(\tilde{u}_2 - U) \cdot \tilde{v}_2} \}/(1+\beta) \tag{25}$$

The second term of (25) is the Reynolds stress which is generated by an ejection motion, and is given by $(\tilde{u}_1(t = T_1) - \tilde{u}_1(t = T)) \cdot \tilde{v}_2$ because this Reynolds stress is equal to the

momentum change of $\tilde{u}$ which is transferred by $\tilde{v}_2 > 0$ during the period of breakdown. Then,

$$\overline{uv} = \frac{1}{(1+\beta)} \{(\overline{\tilde{u}_1 \tilde{v}_1} - \overline{\tilde{u}}_1 \cdot \overline{\tilde{v}}_1) + \overline{\tilde{v}}_1 \cdot (\tilde{u}_1(t=T) - \tilde{u}_1(t=T_1))\} \tag{26}$$

Since $U_*^2 \equiv \nu(\partial \overline{\tilde{u}}/\partial y)_{y=0}$, we can also obtain from (20)

$$U_*^2 \fallingdotseq \nu \frac{1}{T} \int_0^T \left(\frac{\partial \tilde{u}_1}{\partial y}\right)_{y=0} dt = \frac{2}{\sqrt{\pi}} U_0 \sqrt{\frac{\nu}{T}} \tag{27}$$

The above results represent the turbulent characteristics during one bursting period T. However, in order to obtain the actual turbulent characteristics, as compared with the experiments, the probability distribution of T should be taken into account.

Then, the friction velocity (27) by using (10)~(12) becomes as follows:

$$U_*^2 = \int_0^\infty \left(\frac{2}{\sqrt{\pi}} U_0 \sqrt{\frac{\nu}{T}}\right) P_T(T) dT = \frac{2}{\sqrt{\pi}} U_0 \sqrt{\frac{\nu}{T_B}} \cdot \gamma^{-3/4} \tag{28}$$

Also, by doing the variable transformation of $s \equiv \log(T/T_0)/\sigma_0$, (23) becomes

$$U^+ \equiv U_0^+ \Phi(y^+) = U_0^+ \int_{-\infty}^\infty G(s) ds \int_0^1 \text{erf}(\Theta) d\tau \tag{29}$$

where, $G(s) = \frac{1}{\sqrt{2\pi}} \exp(-s^2/2)$, and Θ reads

$$\Theta \equiv \frac{y}{2\sqrt{\nu t}} = \frac{\sqrt{\pi}}{4} \gamma^{1/4} \frac{y^+}{U_0^+} \frac{1}{\sqrt{10^{\sigma_0 s} \cdot \tau}} \tag{30}$$

In the same manner, we can obtain from (24) and (26):

$$\left(\frac{u'}{U_*}\right)^2 = U_0^{+2} \int_{-\infty}^\infty G(s) ds \int_0^1 \{\text{erf}(\Theta)\}^2 d\tau - U^{+2} \tag{31}$$

$$\left(\frac{v'}{U_*}\right)^2 = \frac{\gamma^{1/2}}{(1+\beta)(2\alpha U_0^+)^2} \left[\int_{-\infty}^\infty \frac{G(s)}{10^{\sigma_0 s}} ds \right.$$
$$\left. \times \int_0^1 \frac{(1-\exp(-\Theta^2))^2}{\tau} d\tau + \frac{1}{\beta} \Psi(y^+)\right] \tag{32}$$

$$\frac{-\overline{uv}}{U_*^2} = \frac{\gamma^{1/4}}{(1+\beta) \cdot 2\alpha} \left[\left\{\int_{-\infty}^\infty \frac{G(s)}{\sqrt{10^{\sigma_0 s}}} ds\right.\right.$$
$$\times \int_0^1 \frac{(1-\exp(-\Theta^2)) \cdot \text{erf}(\Theta)}{\sqrt{\tau}} d\tau - \Phi(y^+) \cdot \Psi(y^+)\Big\}$$
$$\left. + \Psi(y^+) \cdot \left\{1 - \text{erf}\left(\frac{\sqrt{\pi}}{4} \gamma^{1/4} \frac{y^+}{U_0^+}\right)\right\}\right] \tag{33}$$

where, $\Psi(y^+) \equiv \int_{-\infty}^\infty \frac{G(s) ds}{\sqrt{10^{\sigma_0 s}}} \int_0^1 \frac{(1-\exp(-\Theta^2))}{\sqrt{\tau}} d\tau$. Lastly, the bursting period T_B is obtained from (28), as follows:

$$\frac{T_B U_*^2}{\nu} = \frac{4\gamma^{-3/2}}{\pi} U_0^{+2} \tag{34}$$

If the parameters α, β, γ (or ψ) and U_0^+ can be chosen suitably, the mean velocity U^+, the turbulence intensities u'/U_* and v'/U_*, the Reynolds stress $-\overline{uv}/U_*^2$ and others will be able to be predicted quantitatively by the present renewal model, though this model is inherently quasi-two -dimensional.

4.3 Turbulent characteristics evaluated by the present renewal model

We here discuss the turbulent characteristics only in the wall region of $y^+ < 50$, where the bursting phenomenon is observed most clearly, as mentioned earlier.

(a) Mean velocity distribution

It has been confirmed by many experiments that the mean velocity distribution U^+ in the wall region can be fairly well given by

$$\frac{dU^+}{dy^+} = \frac{2(1-y^+/R_*)}{1+\sqrt{1+4l^{+2}(1-y^+/R_*)}} \tag{35)}$$

where l^+ is the mixing length proposed by van Driest.[26] It is represented by

$$l^+ = \Gamma \cdot \kappa y^+, \quad \Gamma \equiv 1 - \exp(-y^+/A) \tag{36}$$

in which Γ is the damping factor, and κ and A are experimental constants, i.e. $\kappa = 0.4$ and $A = 27$.

Now, (29) was numerically solved with a zero variance, i.e. $\psi = 0$ and various values of the main stream velocity U_0^+. From the results, it was concluded that (29) showed a good agreement with (35), for $R_* = 500$ when $U_0^+ = 15$.

Next, on condition that $U_0^+ = 15$ and ψ varied up to 2.0, the mean velocity distributions were obtained from (29) and are shown in figure 12. Although U^+ decreases a little as ψ becomes larger, the curves of the present renewal model have a good agreement with those of van Driest, when $U_0^+ = 15$ and $\psi = (0 \sim 1.5)$. Certainly, Black's model shows a better agreement with (35) than the present model, for Black's model has an initial condition closer to the actual phenomenon, as pointed out previously. As y^+ becomes larger than 30, (29) gradually approaches the well-known logarithmic law of Prandtl. On the other hand, as y^+ becomes smaller than 10, (29) gradually approaches the velocity distribution of the viscous sublayer, i.e. $U^+ = y^+$, since erf $\Theta \to 2\Theta/\sqrt{\pi}$ at $y^+ \to 0$.

(b) Turbulent intensities

The distribution of u'/U_* can be calculated easily by using (31) if the values of U_0^+ and ψ are given. The curves of u'/U_*, calculated under the conditions that $U_0^+ = 15$ and $\psi = 0.0 \sim 1.5$, are shown in figure 13, together with the experimental values.[3],[27],[28]
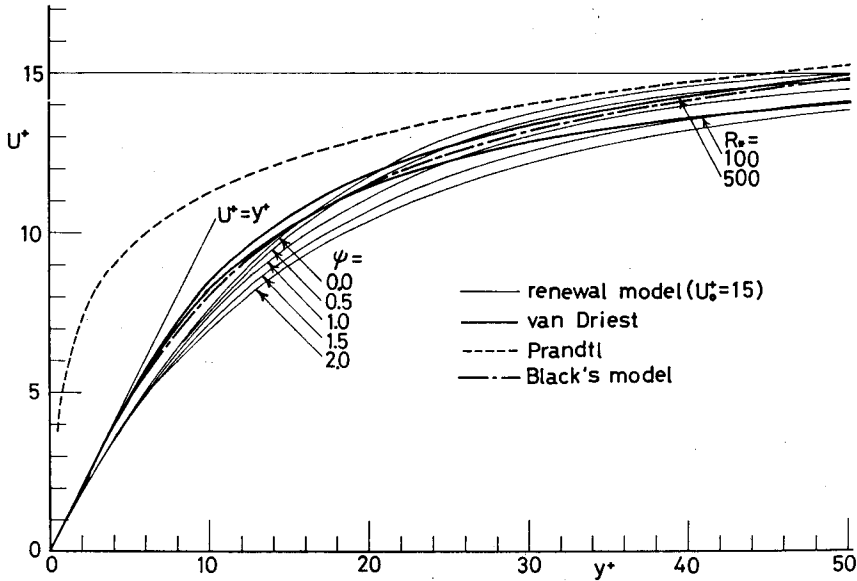
Fig. 12. Mean velocity distributions by the present renewal model
($U_0{}^+=15$ and ψ is varied).

As ψ becomes larger, u'/U_* of (31) increases in the region of $y^+>10$, and the experimental values seem to exist between the curves of $\psi=0.5$ and 1.0, whose results are fairly reasonable as seen in figure 10. The quantitative differences between the calculated and the observed values, however, are fairly large. This difference in the region of $y^+>20$ may indicate that the nonlinear coupling effect and the pressure fluctuation effect cannot be neglected even in the built-up duration. This is because there does'nt actually exist such an idealized bursting phenomenon as described here, and also because the fluctuation of the main stream velocity $U_0{}^+$ should be considered in connection with the behaviours in the equilibrium region. When $y^+\to0$, (31) approaches

$$u'/U_*=B \cdot y^+ + O(y^{+3}) \tag{37}$$

and B becomes about 0.9, which corresponds to three times the experimental value, i.e. $B=0.3$, as seen in figure 13.

Next, in order to calculate (32) for v'/U_*, the parameters α and β must be determined beforehand. It was here decided tentatively that $\alpha=0.7$ and $\beta=0.01$, because α is the order of ($0.7{\sim}0.8$) and β is a very small value. Therefore, the calculated curves of v'/U_* with $U_0{}^+=15$, $\alpha=0.7$, $\beta=0.01$ and a parameter of ψ are also described in figure 13. It should be noticed that the effect of ψ on v'/U_* is very small, and that the calculated curves agree very well with the experimental values, in contrast to u'/U_*. Though this quantitative agreement might be fortuitous, since $\tilde{v}$ was derived logically from $\tilde{u}$, one of the reasons for this agreement might be due to the integral operation of (21). As y^+
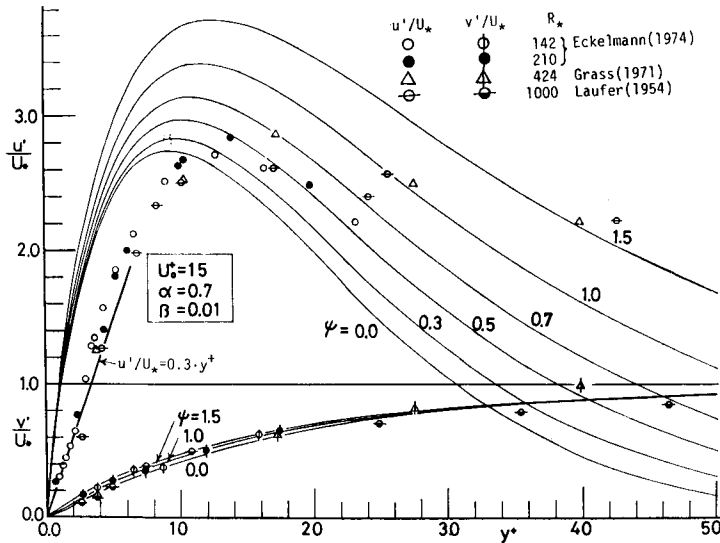
Fig. 13. Turbulence intensities described by the present model
($U_0{}^+=15$, $a=0.7$, $\beta=0.01$ and ψ is varied).

becomes larger, $\hat{u}$ has a weaker relationship with the coherent motion, but $\hat{v}$ always contains all of this motion on an average, that is, the accumulation effect from the wall up to y^+ might give a good result for v'/U_*.

To sum up, it may be concluded that the present renewal model can describe fairly well, even quantitatively, the turbulence intensities in the region of $y^+<30$, though its model has several inherent defects. In particular, this model can satisfactorily explain the remarkable characteristic that u'/U_* has a maximum value at $y^+=(10\sim20)$, although v'/U_* increases monotonously.

(c) Reynolds stress distribution

Since the parameters have been determined so that $U_0{}^+=15$, $a=0.7$, $\beta=0.01$ and $\psi=(0.5\sim1.0)$, the Reynolds stress distribution can be also obtained easily from (33). These calculated results showed a qualitative agreement with the experimental data obtained by Eckelmann,[28] although some quantitative differences as seen in u'/U_* also appeared for $y^+>30$, because this Reynolds stress was evaluated directly from the time-average of $u(t)\times v(t)$.

The mean Reynolds stress $-\overline{uv}$ is also evaluated indirectly from the equation of motion. That is, since

$$\frac{-\overline{uv}}{U_*{}^2}=(1-y^+/R_*)-\frac{dU^+}{dy^+} \tag{38}$$
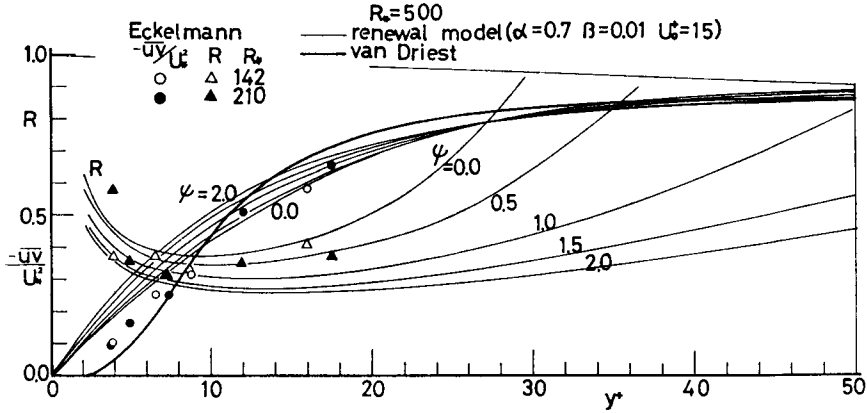
in an open-channel flow, it becomes from (29) as follows:

Fig. 14.   Reynolds stress distribution described by the present model
($U_0^+=15$, $a=0.7$, $\beta=0.01$ and ψ is varied).

$$\frac{-\overline{uv}}{U_*{}^2}=\left(1-\frac{y^+}{R_*}\right)-\frac{\gamma^{1/4}}{2}\int_{-\infty}^{\infty}\frac{G(s)ds}{\sqrt{10^{\sigma_0^s}}}\int_0^1\frac{\exp(-\Theta^2)}{\sqrt{\tau}}\,d\tau \qquad (39)$$

Figure 14 shows the results of (39), van Driest's curve being calculated by using (35) and (38), and Eckelmann's experimental values. The quantitative agreements among them are fairly good.

Also, the correlation coefficients $R=-\overline{uv}/u'v'$, calculated from (31), (32) and (39), are shown in figure 14, compared with Eckelmann's experimental values. This model with $\psi=(0.5\sim1.0)$ gives nearly constant values of R in the buffer layer, i.e. $R=(0.3\sim0.4)$, which agree fairly well with the observed results.

4.4   Explanation of the bursting process by the renewal model

The most outstanding point of the present model is that the instantaneous velocity profiles $\tilde{u}(t)$ and $\tilde{v}(t)$ can be approximately estimated, and thus the bursting process can be explained quantitatively, as follows.

Firstly, figure 15 shows the instantaneous velocity profiles $\tilde{\boldsymbol{u}}=(\tilde{u},\,\tilde{v})$ at each time $\tau=t/T$ in one bursting period, which have been calculated from (20)$\sim$(22) on the conditions that $U_0^+=15$, $a=0.7$ and $\beta=0.01$, as decided in the previous section. In the early stage when τ is small, the sweep motion occurs and the acceleration flow $(u>0)$ penetrates the buffer layer $(v<0)$. The profile of $\tilde{u}(\tau)$ is gradually strained with the time elapsed, and it nearly coincides with the mean velocity distribution at $\tau=0.5$, which corresponds to a half of the bursting period. Then, $\tilde{u}(\tau)$ turns into the deceleration flow $(u<0)$ and is further strained. Immediately after the velocity-strain has reached the critical maximum value, the coherent motion or the horseshoe vortex breaks down in a short time $(\beta=0.01)$, and then the stress-relieved mechanism or the turbulence production occurs. Consequently, the high turbulent stressed energy is released outwards $(v_2>0)$
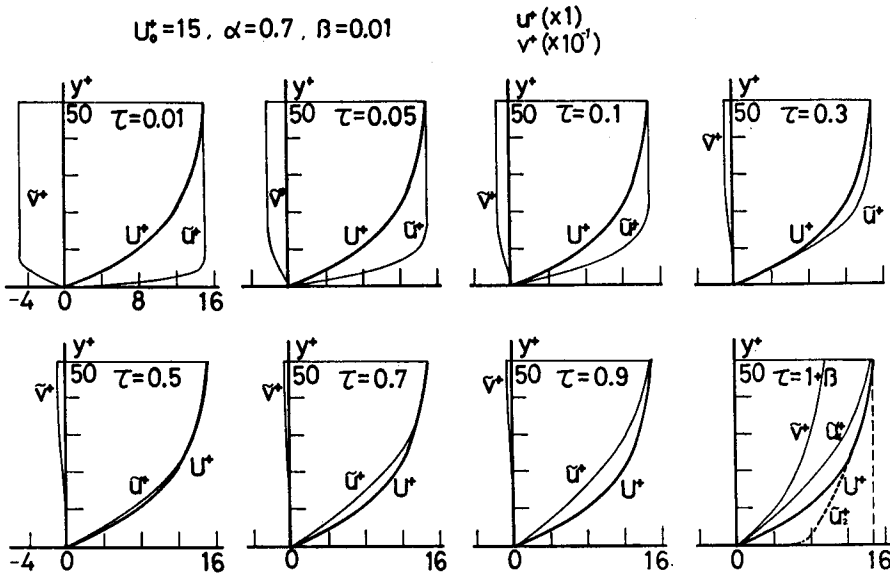
Fig. 15. Instantaneous velocity profiles $\bar{u}^+$ and $\bar{v}^+$ in one bursting period
evaluated by the present model.

by this ejection motion. After this breakdown period, a new build-up stage starts again. Such a sequent behavior of the instantaneous velocity profile may coincide very well with Corino & Brodkey's observation (figure 1) or Hinze's conceptual model (figure 11).

Next, the distributions of instantaneous Reynolds stress obtained as $w(t) \equiv u(t) \times v(t)$ are shown in figure 16. We can discuss here the characteristics of $w(t)$ at least up to the buffer layer, because the present model is not fully applicable to the region of $y^+ > 30$, as mentioned previously. In the duration up to $\tau \simeq 0.1$, the sweep event exists and the positive Reynolds stress is generated. The horseshoe vortex during $0.1 < \tau < 1.0$ contributes little to the production of Reynolds stress, and especially, the interaction event appears when $\tau > 0.5$. During the period of the vortex-breakdown, i.e. $(1+\beta)^{-1} < \tau < 1$, the ejection motion generates the positive Reynolds stress enormously and violently. It should be noted that the maximum production of the Reynolds stress occurs at $y^+ = (10\sim20)$, which corresponds closely to the position of the maximum turbulence intensity u'/U_*, as shown in figure 13.

In detailed discussion, the fraction of time occupied by ejection and sweep motions becomes nearly equal to 0.1, according to the present model. This result coincides fairly well with the experimental data[10] evaluated at the discrimination level $H \simeq 5$, where both of these motions may be detected in the hot-film signals as mentioned in chapter 3. Figure 16 also shows that the ejection motion in the buffer layer has such a pulse-like behaviour that uv/U_*^2 attains to about 40 in the very short time of $\beta = 0.01$, similar to the hot-film signals in figure 2. According to this model, the contribution to
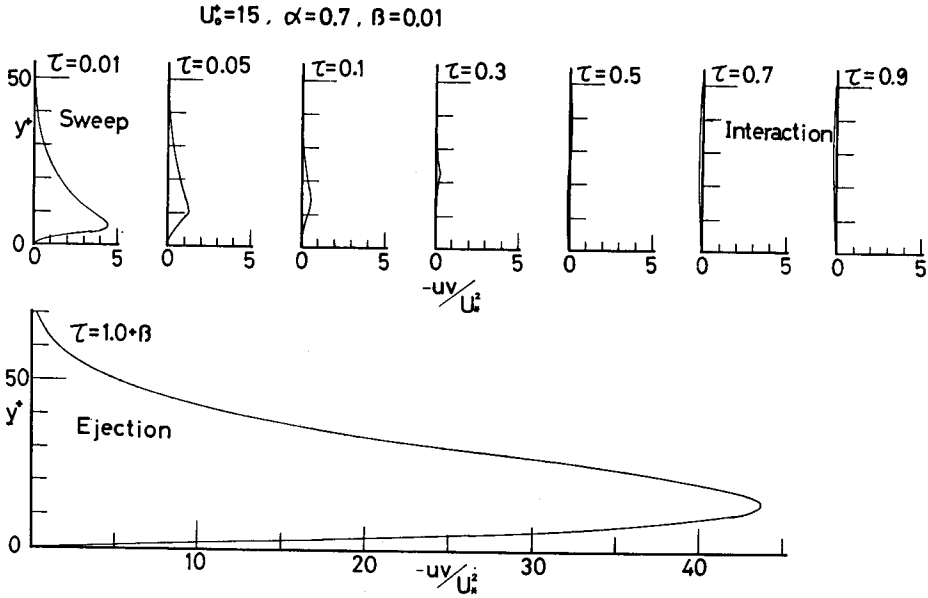
Fig. 16.   Instantaneous Reynolds-stress profiles near the wall in one bursting
period evaluated by the present model.

$-\overline{uv}/U_*{}^2$ becomes close to $40\beta = 0.4$ at the ejection, and 0.2 at the sweep.   Consequently,
$RS_2 \equiv \overline{w_2(t)} \doteqdot 0.67$ and $RS_4 \equiv \overline{w_4(t)} \doteqdot 0.33$ are obtained since $-\overline{uv}/U_*{}^2 = 0.6$.   Because
the present model can't describe satisfactorily the interaction events which probably
correspond to the nonlinear effect, these estimated values show some differences from
the experimental data of $RS_2 \doteqdot 0.77$ and $RS_4 \doteqdot 0.57$.[10]

Lastly, we discuss the bursting period T_B evaluated by the renewal model.   When
$U_0{}^+ = 15$ and $\psi = (0.5 \sim 1.0)$, (34) becomes $T_B U_*{}^2/\nu = (300 \sim 400)$, which corresponds to
$R_* = (3500 \sim 5000)$, as judged from figure 8.   The magnitude of this Reynolds number
may not be so unreasonable, though it is a little large for the usual experiments.

Now, assuming that an average strain in the $\bar{u}$-distribution or its instability can be
expressed by the average value $\bar{\delta}_*$ of its displacement thickness, we can obtain

$$\bar{\delta}_* = \int_0^T p_T(T)dT \int_0^1 d\tau \int_0^\infty \left(1 - \frac{\bar{u}^+}{U_0{}^+}\right)dy = \frac{4}{3}\sqrt{\frac{\nu T_B}{\pi}}\gamma^{1/4} \tag{40}$$

$$\left.\begin{array}{l} \dfrac{\bar{\delta}_* U_0}{\nu} = \dfrac{8}{3\pi}\gamma^{-1/2}U_0{}^{+2} \\[2mm] \dfrac{\bar{\delta}_* U_*}{\nu} \equiv \bar{\delta}_*{}^+ = \dfrac{8}{3\pi}\gamma^{-1/2}U_0{}^+ \end{array}\right\} \tag{41}$$

Since it is approximated that $Re \simeq \delta U_0/\nu \simeq 8 \cdot \bar{\delta}_* U_0/\nu$ by making use of the 1/7-power
velocity law, the Reynolds number Re becomes $(1600 \sim 1800)$ when $U_0{}^+ = 15$ and $\psi = (0.5 \sim 1.0)$.   Consequently, this Reynolds number nearly corresponds to the critical

number which represents the instability of the sublayer or buffer layer. Then, we can also obtain $\overline{\delta}_*{}^+=(13\sim15)$, which corresponds to the edge of the sublayer. These results may confirm more or less a previous suggestion that the occurrence of the bursting phenomenon may be due to an instability of the flow near the edge of the sublayer, whereby the bursting phenomenon may have a strong resemblance to the mechanism of a laminar-turbulent transition.

5. Conclusions

In the present study, we firstly proposed a new evaluation method for the bursting period on the basis of the phenomenological consideration that the number of occurrences of interaction-like motions should be removed from those of the ejection or sweep events in the sorted Reynolds-stress fluctuating signals. The periodic characteristics of the bursting phenomenon in open-channel flows have been evaluated definitely by this method, and the effects of the Reynolds and the Froude numbers as well as the wall roughness upon the bursting period have been systematically investigated. Consequently, the following noticeable results have been confirmed even in open-channel flows, as well as in boundary layer flows. That is, the mean bursting period or the streamwise spatial scale of a horseshoe vortex may be universally expressed by outer rather than inner parameters, and its probability distribution becomes log-normal. On the other hand, the transverse spatial scale of this vortex may scale with inner rather than outer parameters. Thus, it has been suggested that the bursting phenomenon might be controlled self-consistently by both the inner and outer parameters. In other words, it might be closely related to the breakdown mechanism of both the macro- and micro-scale eddies.

Next, in order to explain even quantitatively the bursting process or the turbulent structure in the wall region, we proposed a simple simulated model which is called a renewal model, on the basis of the Einstein-Li model and also the knowledge of the bursting-period characteristics obtained above. Though the present model was inherently quasi-two-dimensional and quasi-linear, this model could describe fairly well, even quantitatively, some distributions of mean-velocity, turbulence intensities and the mean Reynolds stress in the wall region. In particular, we showed the noticeable result that the present model could satisfactorily explain a sequence of the bursting process or a mechanism of the turbulence-production near the wall, though its quantitative explanation might be rough more or less.

References

1) Kline, S. J., Reynolds, W. C., Schraub, F. A. and Runstadler, P.W.: J. Fluid Mech., **30**, 741 (1967).

2) Corino, E. R. and Brodkey, R. S.: J. Fluid Mech., **37**, 1 (1969).

3) Grass, A. J.: J. Fluid Mech., **50**, 233 (1971).

4) Kim, H. T., Kline, S. J. and Reynolds, W. C.: J. Fluid Mech., **50**, 133 (1971).

5) Nychas, S. G., Hershey, H. C. and Brodkey, R. S.: J. Fluid Mech., **61**, 513 (1973).

6) Offen, G. R. and Kline, S. J.: J. Fluid Mech., **62**, 223 (1974).

7) Offen, G. R. and Kline, S. J.: J. Fluid Mech., **70**, 209 (1975).

8) Lu, S. S. and Willmarth, W. W.: J. Fluid Mech., **60**, 481 (1973).

9) Brodkey, R. S., Wallace, J. M. and Eckelmann, H.: J. Fluid Mech., **63**, 209 (1974).

10) Nakagawa, H. and Nezu, I.: J. Fluid Mech., **80**, 99 (1977).

11) Rao, K. N., Narasimha, R. and Narayanan, M. A. B.: J. Fluid Mech., **48**, 339 (1971).

12) Lu, S. S. and Willmarth, W. W.: Phys. of Fluids, **16**, 2012 (1973).

13) Laufer, J. and Narayanan, M. A. B.: Phys. of Fluids, **14**, 182 (1971).

14) Sabot, J. and Comte-Bellot, G.: J. Fluid Mech., **74**, 767 (1976).

15) Nezu, I.: *Turbulent structure in open-channel flows, Ph.D thesis in Civil Engineering, Kyoto University* (1977) (in Japanese).

16) Nakagawa, H. and Nezu, I.: *5-th Symposium on Flow Visualization, I.S.A.S. Univ. of Tokyo,* No. 5, p. 47, (1977), (in Japanese).

17) Hinze, J. O.: *Turbulence* (*2-nd ed.*), McGraw-Hill, (1975).

18) Sandborn, V. A.: J. Fluid Mech., **6**, 221 (1959).

19) Ueda, H. and Hinze, J. O.: J. Fluid Mech., **67**, 125 (1975).

20) Gurvich, A. S. and Yaglom, A. M.: Phys. of Fluids, **10**, S59 (1967).

21) Theodorsen, T.: *50 Jahre Grenzschichtforschung,* (*ed. by Görtler, H. and Tollmien, W.*) *Friedr. Vieweg & Sohn, p.* 55 (1955).

22) Einstein, H. A. and Li, H.: Proc. Amer. Soc. Civ. Engrs., EM-2, p. 1 (1956).

23) Willmarth, W. W. and Tu, B. J.: Phys. of Fluids, **10**, S134 (1967).

24) Black, T. J.: *AIAA* **6***-th Aero. Sci. Meeting, AIAA Paper No.* 68–42. (1968).

25) Nakagawa, H. and Nezu, I.: Proc. Japan Soc. Civ. Engrs., No. 231, p. 61 (1974).

26) van Driest, E. R.: J. Aero. Sci., **23**, 1007 (1956).

27) Laufer, J.: NACA TR-1174 (1954).

28) Eckelmann, H.: J. Fluid Mech., **65**, 439 (1974).